Nanoscale

Accepted Manuscript

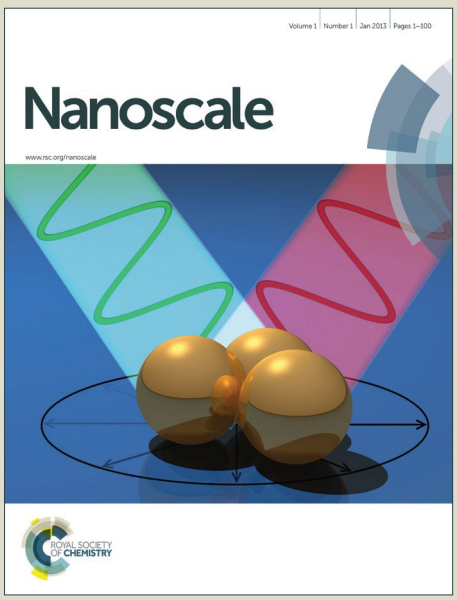

ROYAL SOCIETY OF CHEMISTRY

www.rsc.org/nanoscale

On the Study of Surface Capping Role on Energy Transfer in Metal Cluster-Semiconductor Nanocomposites

Dipankar Bain,[†] Bipattaran Paramanik,[†] Suparna Sadhu[#] and Amitava Patra[*†]

[†]Department of Materials Science, Indian Association for the Cultivation of Science, Kolkata 700 032, India

[#] Department of Chemistry, Sukumar Sengupta Mahavidyalaya, Keshpur, Paschim Medinipur, WB, India

[*]Author to whom correspondence should be addressed. Electronic mail: msap@iacs.res.in. Telephone: (91)-33-2473-4971. Fax: (91)-33-2473-2805.

Abstract

Metal cluster-semiconductor nanocomposite materials remains a frontier area of research for the development of optoelectronic, photovoltaic and light harvesting devices because metal nanoclusters and semiconductor QDs are promising candidates for photon harvesting. Here, we have designed well defined metal cluster-semiconductor nanostructures using different surface capped negatively charged Au_{25} nanoclusters (Au NCs) and positively charged cysteamine capped CdTe quantum dots by electrostatic interaction. The main focus of this article is to address the impacts of surface capping agents on the photophysical properties of Au cluster-CdTe QDs hybrid nanocomposites. Steady state and time resolved spectroscopic studies reveal that photoluminescence quenching, radiative and nonradiative rate, energy transfer between Au nanoclusters and CdTe QDs have been influenced by the nature of capping agent. We have calculated the energy transfer related parameters like overlap integral, distance between donor and acceptor, Förster distance, efficiency of energy transfer and rate of energy transfer from CdTe QDs to three different Au NCs. Photoluminescence quenching varies from 73 % to 43% with changing the capping agents from bovine serum albumin (BSA) to glutathione (GSH). The efficiency of energy transfer from CdTe QDs to BSA-capped Au NCs is found 83%, for Cys-capped Au NCs 46% and for GSH-capped Au NCs 35% which depends on the number of Au cluster attached to per QD. It reveals that the nature of capping ligands plays a crucial role for the energy transfer phenomena from CdTe QDs to Au NCs. Interesting findings reveal that the efficient energy transfer in metal cluster-semiconductor nanocomposites may open up new possibilities in designing of artificial light harvesting system for future applications.

Introduction:

The size and shape controlled metal nanoclusters (NCs) has drawn a considerable research interest due to their tremendous applications in optics, biology, catalysis and biomedicine.[1-5] Gold nanoclusters (Au NCs) are ultrasmall particles below 2 nm size; consist of several to hundred gold (Au) atoms.[6, 7] The properties of metal nanoclusters (NCs) are controlled by their subnanometer dimension, are far different from those bulk materials and nanoparticles.[8, 9] Unlike nanoparticles (NPs), the density of states in NCs is not enough to exhibit shape and size dependent surface plasmon resonance (SPR).[10-12] Due to strong quantum confinement, nanoclusters exhibits molecular like properties, such as d-sp and sp-sp transition, intense fluorescence and intrinsic magnetism.[13, 14] The photoluminescence (PL) wavelength of metal NCs can be tuned from near infrared (NIR) to ultraviolet (UV), either by changing the number of core atoms within the cluster or varying the capping ligands of clusters.[7, 15, 16] The stability and solubility of noble metal NCs are totally governed by the capping ligands.[9] Most commonly used capping ligands containing -SH, -NH_2 and -COOH groups are used owing to their higher solubility in aqueous medium.[9] Phosphorus and oxygen capped NCs are generally insoluble in water, restricts is wide applicability. Noteworthy, thiol (-SH) has very strong affinity with NCs due to soft-soft interaction.[17-19] Thus, thioalcohols, thioacids and sulfur containing amino acids or peptides are widely used for water soluble metal cluster synthesis. Highly fluorescent Ag NCs has been synthesized by Dickson and his coworkers, using PAMAM dendrimer cage.[20] Biopolymers such as DNA or different proteins are being used for the synthesis of Ag, Au even Cu NC.[21-25] Recently, a multi-thiol based ligand like dihydrolipoic acid (DHLA) have used for the synthesis of stable NIR emissive Au NCs by Nienhaus and co-workers[26]. Later, Mattoussi *et al*.[27, 28] have demonstrated the incorporation of zwitterionic anchor can enhance the photophysics (QY, decay time etc.) and stability of the DHLA capped Au NCs or Ag NCs. Jin and his coworkers have been reported that the surface ligands influence the fluorescence property of gold nanoparticles.[29] The surface ligand can influence the fluorescence properties of metal nanoparticles in two different ways one is charge transfer from ligands to metal nanoparticle core (LMNCT) through Au-S bonds and another one is electron donation from electron rich atom of ligands to metal core.[29] Prashant V. Kamat *et al*. [30] have elaborated how gold cluster acts as sacrificial electron donor to generate hydrogen gas, in presence of short band gap semiconducting quantum dots. Recently, Maran *et al*.[31] have studied that the electron transfer

process is influenced by ligand's chain length in monolayer-protected clusters (MPCs). A new class of metal cluster-semiconductor nanocomposites has been paid a great attention recently because of their complementary optical properties of long-lived excitations in semiconductor and tunable optical properties in metal nanoclusters.[32-34] The combination of these optical properties provides attractive opportunities to design new materials for photonic applications. Less attention has been paid on fundamental understanding of photophysical properties of metal cluster-semiconducting nanoparticles nanocomposites by using spectroscopy.

In the present study, we have synthesized positively charged cysteamine capped CdTe QDs and three negatively charged Au NCs using aqueous phase method. All the nanoclusters are consisting of 25 gold atoms (Au_{25}) with varying the capping ligands to understand the influence of capping agents on the photophysical properties of Au cluster-CdTe QDs nanocomposites. Various characterization methods like absorption spectroscopy, photoluminescence (PL) spectroscopy, transmission electron microscope (TEM), X-ray photoelectron spectroscopy (XPS), and matrix assisted laser desorption ionization-time of flight (MALDI-TOF) mass spectrometry have been used to characterize the Au cluster-CdTe QDs nanocomposites. The quenching of fluorescence intensity of CdTe QDs in nanocomposites has been investigated by steady state and time resolved fluorescence spectroscopy. Au clusters act as energy acceptor whereas CdTe QDs act as energy donor because the emission spectrum of CdTe QD matches well with the absorption spectrum of Au clusters. Analysis suggests that an efficient energy transfer (ET) occurs from CdTe QDs to Au NCs. We have also noticed the drastic changes in energy transfer rate constant, quantum yield (QY) and decay time of CdTe QDs in nanocomposites occur with changing the capping ligands of the Au NCs. Therefore, the photophysical interactions between Au NCs and CdTe QDs in nanocomposites are governed by the capping ligand of the Au NCs.

Experimetal scetion

Materials

Tellurium powder, cadmium chloride hemi-pentahydrate ($CdCl_2 \cdot 5/2H_2O$), tetrachloroauric acid ($HAuCl_4.3H_2O$), glutathione reduced (GSH), 2, 5-dihydroxybenzoic acid (DHB), Cysteamine and L-Cysteine (Cys) were obtained from Sigma-Aldrich. Other chemicals such as sodium hydroxide (NaOH), sodium borohydride ($NaBH_4$), and bovine serum albumin (BSA) were received from Merck. Dialysis tube (molecular weight cut off <12KDa) was

purchased from Fischer Chemicals. Millipore deionized water (18.2 MΩ) was used for solution preparation in this study. All the chemicals of highest purity grade were used without further purification.

Synthesis of BSA Capped gold nanoclusters (Au NCs)

Au NCs capped by BSA was synthesized following the standard method.[35] Aqueous $HAuCl_4$ solution (1 mL, 10 mM) was added to a BSA solution (1mL, 50mg/mL) under vigorous stirring for two minutes. Aqueous solution of NaOH (100 µL, 1M) was introduced to make the solution alkaline (pH≈11), and the mixture was incubated at 37 °C for 12 h. The color of the reaction mixture changed from light yellow to light brown, finally to deep brown. The solution of nanocluster was dialyzed (molecular cut off <12KDa) for 6 hours, during the dialysis the water was replaced at 2 hour intervals. The resulting nanocluster solution was stored at 4^0C for further analysis.

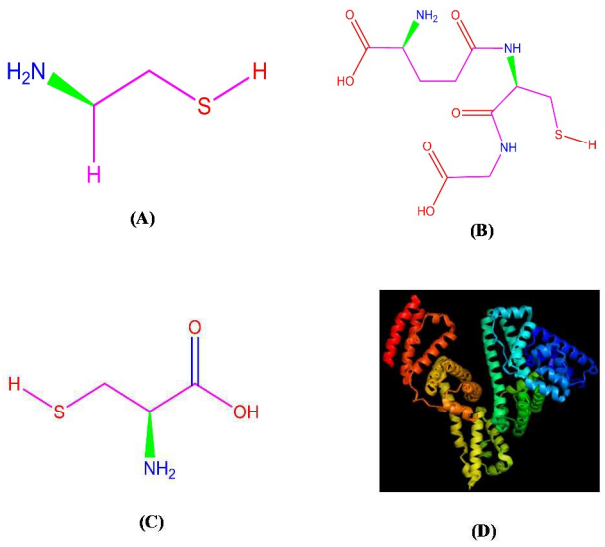

Scheme 1 Chemical structures of (A) cysteamine, (B) glutathione reduced, (C) L-cysteine and ribbon structure of (D) bovine serum albumin (BSA) protein.

Synthesis of highly luminescent Cysteamine-capped CdTe QDs

Cysteamine capped CdTe QDs was synthesized following earlier procedure with some modification.[36-38]

Preparation of NaHTe:

In a typical experiment, Te powder (0.05 mM) was added to O_2-free Millipore water (1.5 mL) in a round bottom flask. The mixture was allowed to stir for 5-7 min to make uniform dispersion of Te powder. The solution of $NaBH_4$ (0.26 mM) was added to the mixture and vigorous stirring was continued. After 1 hour, color of the solution changed to faint pink. The faint pink color became dark and then darker with time, conformed the formation of fresh NaHTe. An argon atmosphere was maintained throughout the experiment to resist the oxidation of highly reactive NaHTe.

Preparation of the cadmium precursor:

Cadmium precursor was prepared by dissolving cadmium chloride hemi-pentahydrate (0.1 mM) in millipore water (25 mL). After 2 min of stirring, Cysteamine (0.24 mM) was added to the Cd^{2+} salt solution under vigorous stirring. Argon gas was bubbled to achieve O_2-free conditions. Then pH of the solution was adjusted to 5.5 by adding HCl (1M). Then, previously prepared NaHTe was immediately injected into the Cd^{2+} solution. This mixture solution was stirred at room temperature for another 45 min under an argon atmosphere. Finally, the solution was heated at 110^0C under argon-purged conditions because CdTe QDs synthesized in inert atmosphere (say N_2 or Ar) acquired lower QY than the CdTe QDs prepared in open air conditions, when keeping the others parameter same. The emission wavelength of the CdTe QDs could be tuned by changing the heating time, that is, growth time of 15, 30, and 45 min. These nanocrystals were stored at 4 °C for further experiment. The final concentration of CdTe QDs was fixed at 1.87 x 10^{-5} M for our experiments.[39]

Preparation of nanocomposite by CdTe QDs and Au NCs:

A series of solution were prepared by mixing CdTe (100 μL) with desired amount of each Au NCs separately. Then, each sample solution was diluted to 3 mL by adding required amount of millipore water. Samples were incubated at 25^0C for 5 minutes with occasional stirring for nanocomposites formation. These incubated samples were used for spectroscopic investigation. Nanocomposites of CdTe QDs with GSH, Cys, and BSA-capped Au NCs are abbreviated as GSH-Au_{25}NC-QD, Cys-Au_{25}NC-QD, and BSA-Au_{25}NC-QD throughout this article.

Characterization

Room-temperature optical absorption spectra were recorded with a UV-vis spectrophotometer (Shimadzu) using a cuvette with a path length of 1 cm. The emission spectra of all of the samples were obtained with a Fluoro Max-P (HORIBA Jobin Yvon) luminescence spectrophotometer. The quantum yield (QY) of CdTe QDs and Au NCs were measured using rhodamine 6G as reference dye. Zeta potential was measured with a Malveron Zetasizer instrument. Transmission electron microscopy (TEM) images and energy dispersive spectroscopy (EDS) spectra were obtained using a JEOL-JEM-2100F transmission electron microscope. The XPS measurements were carried out using an Omicron Nanotechnology instrument. The mass of the NCs were also measured by matrix-assisted laser desorption ionization-time of flight (MALDI-TOF) mass spectrometry on a Bruker Daltonics Autoflex II TOF/TOF system. A pulse laser of 337 nm was used and a saturated CHCA and DHB solution was selected as the matrix for the MALDI-TOF measurements. Fourier-transform infrared (FTIR) spectroscopy measurements were performed on a SHIMADZU made FTIR-8300 Spectrometer using KBr pellets. For time correlated single photon counting (TCSPC) measurement, the samples were excited at 375 nm by picoseconds NANO-LED IBH-375. The fluorescence decays were collected on a Hamamatsu MCP photomultiplier. Equation (1) was used to analyze the experimental time-resolved fluorescence decays, P(t):[40]

$$P(t) = b + \sum_{i}^{n} \alpha_i \exp\,(-t/\tau_i) \qquad (1)$$

Here, n is the number of emissive species, b is the baseline correction ("DC" offset), and α_i and τ_i are, respectively, the pre-exponential factor and the excited-state fluorescence decay time associated

with the ^{i}th component. The average decay time, $< \tau >$, was calculated from following equation.

$$\langle \tau \rangle = \sum_{i=1}^{n} a_i \tau_i \qquad (2)$$

Where $a_i = \alpha_i / \sum \alpha_i$ and is the contribution of the decay component.

The quantum yield (QY) of all samples were obtained by comparison with reference dye, rhodamine 6G (in water), using the following equation.

$$QY_s = (F_s \times A_r \times \eta_s^2 \times QY_s) / (F_r \times A_s \times \eta_r^2) \qquad (3)$$

Where, F_s and F_r are the integrated fluorescence emission of the sample and the reference. A_s and A_r are the absorbance at the excitation wavelength of the sample and the reference. QY_s and QY_r are the quantum yields of the sample and the reference (QY_r = 0.95). The refractive indices of the solvents used for the preparation of the sample and reference are given by n_s (1.33) and n_r (1.33), respectively (here both solvents are water).

Results and discussion

Structural characterization

Transmission electron microscope (TEM), matrix assisted laser desorption ionization (MALDI), X-ray photoelectron spectroscopy (XPS), Fourier transform infrared spectroscopy (FTIR) are used to characterize the morphology of synthesized Au NCs. Fig. 1 shows the HRTEM images of Au clusters capped by different capping ligands and the average size of Au NCs obtained from particle size distribution are 1.70, 1.50, and 2.0 nm for GSH-, Cys- and BSA-capped Au NCs, respectively.

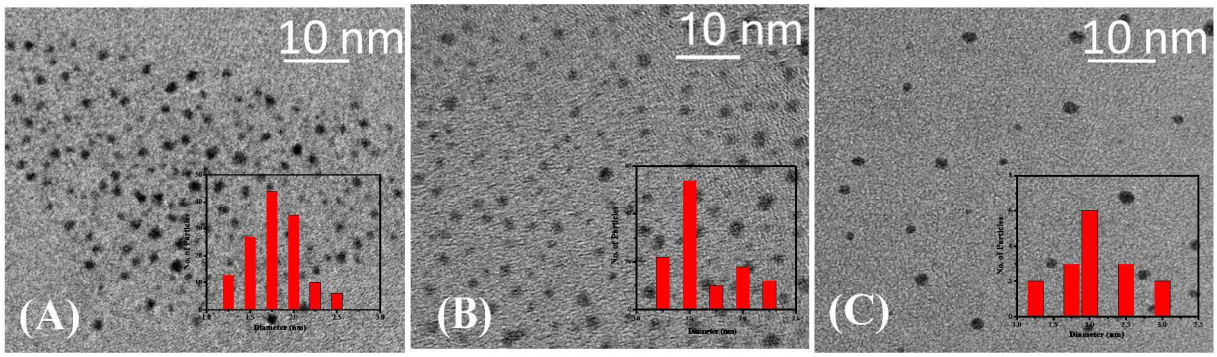

Fig. 1 TEM images of Au nanoclusters capped by (A) GSH, (B) Cys, and (C) BSA.

To estimate the exact molecular mass of as prepared Au NCs, matrix-assisted laser desorption/ionization-time of-flight (MALDI-TOF) mass spectrometry is performed. The MALDI-TOF spectrum of GSH capped Au NCs shows peak at m/z~10110.29 Da which is well fitted with the calculated mass of Au NCs capped by GSH (Fig. 2A). The MALDI-TOF spectrum of GSH capped Au NCs reveals that Au NCs consist 18 GSH molecules to capped 25 atoms of Au, also supported by the previous report.[41] Similarly, the MALDI-TOF spectrum of Cys capped Au NCs shows peak at m/z~6869.65 Da which is well matched with the calculated mass of Au NCs capped by Cys (Fig. 2B). The MALDI-TOF spectrum of Cys capped Au NCs

confirms that the Cys capped Au NCs contains 18 Cys molecules to capped 25 Au atoms, also suggested by the earlier report.[41]

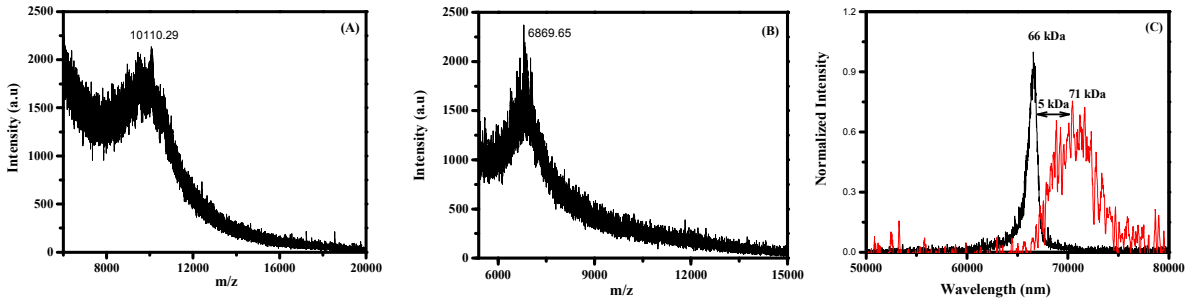

Fig. 2 MALDI-TOF spectra of Au nanoclusters capped by (A) GSH, (B) Cys, and (C) pure BSA protein (black) and BSA–Au NCs (red).

The mass of pure BSA protein obtained from MALDI-TOF spectrum is about 66 kDa, but the mass of BSA capped Au NCs is observed at m/z~ 71 kDa (Fig. 2C). The shifting of peak (around 5 kDa) is due to the formation of BSA capped Au_{25} nanoclusters, suggested by the previous report.[35] Here, one BSA molecule is enough to capped 25 Au atoms because of its larger size compared to GSH and Cys. Thus, MALDI-TOF analysis confirms that core of all the Au NCs consist 25 Au atoms though the capping ligands are different.

Further, X-ray photoelectron spectroscopy (XPS) analysis has been performed to understand the bonding nature between ligand and metal in Au NCs. Here, we have find out the oxidation states of Au in GSH-Au_{25}NC.

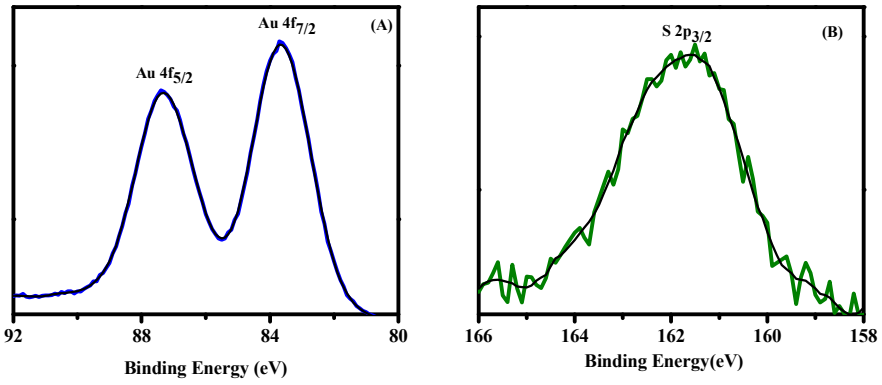

Fig. 3 XPS spectra for the elements, Au (A) and S B) of GSH-Au_{25}NC.

The binding energies of $4f_{7/2}$ and $4f_{5/2}$ are 83.66 eV and 87.28 eV, respectively (Fig. 3A). The shifting of $4f_{7/2}$ with respect to bulk Au^0 and Au^+ confirms the formation of Au NCs and does not matches with Au^0 or Au^I.[41] Therefore, the co-existence of Au^0 and Au^+ states is also a special characteristic of Au NCs, as suggested by the earlier report.[42] The de-convolute XPS curve shows that the binding energy of S $2p_{3/2}$ is 161.58 eV, which is consistent with previous reports (Fig. 3B).[42]

In the absorption study of Au NCs, the absorption band around 670 nm is observed in Cys and GSH capped Au clusters. This absorption band is due to intra-band (sp to sp) electronic transition.[13] The BSA capped Au NCs exhibit blue shifted shoulder at~510 nm,[43] which is due to the mixing of (sp to sp) and (d to sp) intra-band transition (Fig. 4A). Interestingly, BSA-Au_{25}NCs shows intense red emission under excitation at 365 nm (Fig. 4B). The emission maxima for BSA capped Au NCs is 640 nm and the quantum yield is found to be 6% which is consistent with the previous result.[35] Noteworthy, the absorption peak at 520 nm corresponds to the surface plasmon resonance, which is absent in present study.[44-46] The absence of surface plasmon peak suggests the formation of Au NCs. The concentration of Au NCs is calculated by using the molar extinction coefficient at 420 nm (ε_{420} = 112000 cm^{-1} M^{-1}), like previous reports.[47]

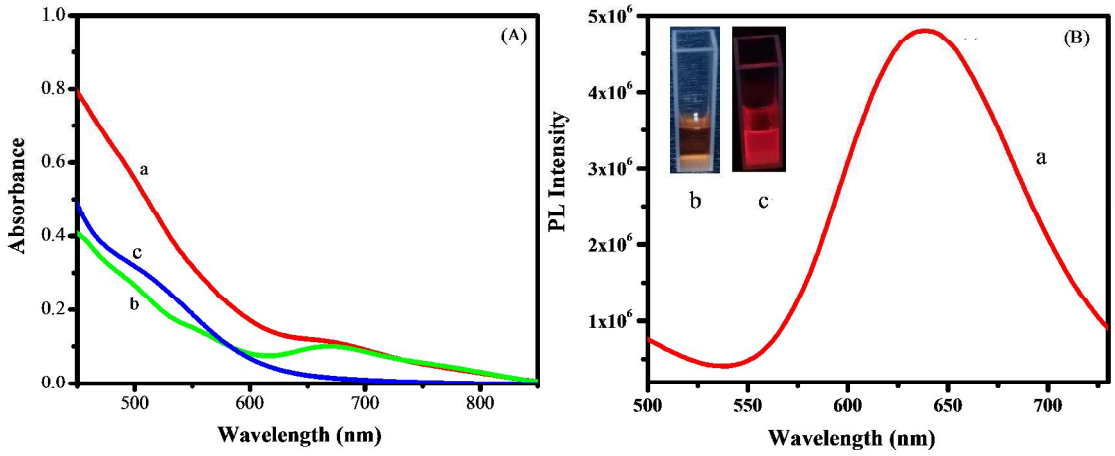

Fig. 4 (A) UV-visible absorption spectra of Au clusters capped by (a) GSH, (b) Cys, and (c) BSA. (B) Photoluminescence spectrum of BSA capped Au NCs (a) and the inset shows the digital photographs of the solution under normal (b) and UV light (c), respectively.

Again, we have synthesized positively charged cysteamine capped CdTe quantum dots in aqueous phase method. The amine end of the cysteamine enhances the solubility of the CdTe

QDs and the thiol end interacts with the CdTe QDs via Cd-S bond formation. The TEM image depicts spherical shape of CdTe QDs with an average size about 3.5 nm which is consistent with the previous reported value (Fig. S1 in ESI†).[38]

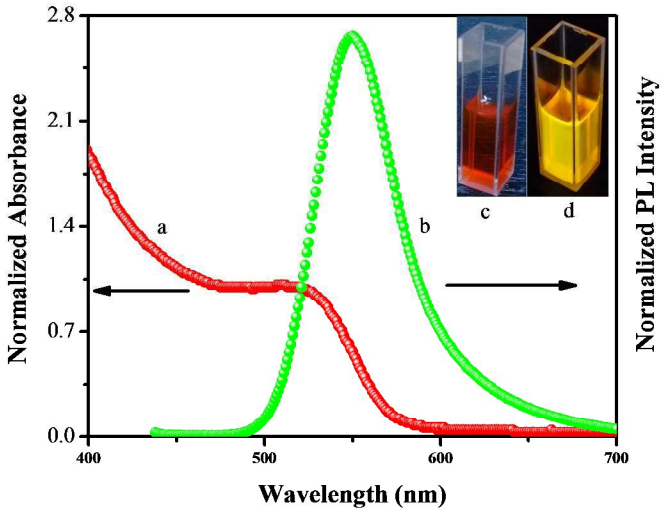

Fig. 5 Absorption spectrum (a) and photoluminescence spectrum (b) of cysteamine capped CdTe quantum dots and the inset shows the digital photographs of the solution under normal (c) and UV light (d), respectively.

The absorption and emission spectrum of cysteamine capped CdTe QDs are shown in Fig. 5. We have observed a broad absorption shoulder at 526 nm and the corresponding emission maxima is observed at 550 nm for cysteamine capped CdTe QDs. The CdTe QDs shows yellow emission under the expose of UV light (inset of Fig. 5) and the QY of CdTe QDs is very low 1.35 %, which is consistent with the previous result.[37] These spherical luminescent CdTe QDs are used for nanocomposites formation with Au NCs where Au NCs consist of 25 gold atoms with varying the capping ligands.

The zeta potential values are -21.2 mV, -40.0 mV, and -32.4 mV (Fig. S2 in ESI†) for GSH-Au_{25}NC, Cys-Au_{25}NC, and BSA-Au_{25}NC, respectively (Table 1), indicating highly negative charged surface of Au NCs. The zeta potential value of CdTe QDs was found to be +33.1 mV (Fig. S2 in ESI†), indicating the highly positive charge surface of CdTe QDs. Therefore, the nanocomposite could be prepared through the electrostatic force of attraction by the positively charged CdTe QDs and negatively charged Au NCs.

Table 1 Zeta potential data of different samples

Sample	Zeta potential/mV
GSH-Au_{25}NC	-21.2 mV
Cys-Au_{25}NC	-40.0 mV
BSA-Au_{25}NC	-32.4 mV
CA-CdTe-QD	+33.1 mV
GSH-Au_{25}NC-QD	+17.8 mV
Cys-Au_{25}NC-QD	+19.5 mV
BSA-Au_{25}NC-QD	-13.2 mV

Here, three different sets of nanocomposites are prepared by using cysteamine capped CdTe QDs with GSH-Au_{25}NC, Cys-Au_{25}NC, and BSA-Au_{25}NC. The zeta potential of GSH-Au_{25}NC-QD nanocomposite is +17.8 mV (Fig. S2A in ESI†), and +19.5 mV (Fig. S2B in ESI†) for Cys-Au_{25}NC-QD nanocomposite. However, the zeta potential for BSA-Au_{25}NC-QD nanocomposite is -13.2 mV (Fig. S2C in ESI†), relatively positive compared to BSA-Au_{25}NC, which confirms the attachment of positive charged CdTe QDs with negative charged Au NCs. The zeta potential of all the nanocomposites is found to be positive compared to Au NCs. Thus, the zeta potential value suggests the formation of nanocomposite in the present study. Fig. 6A depicts the TEM image of BSA-Au_{25}NC-QD nanocomposite, which suggests the attachment spherical CdTe QDs with BSA capped Au NCs and this is further supported by the EDX elemental analysis (Fig. 6B). Similarly the TEM image GSH-Au_{25}NC-QD nanocomposite reveals the attachment of positively charged CdTe QDs with negatively charged Au NCs owing to electrostatic interaction (Fig. S3A in ESI†). The distinct peaks for Au, S, Cd and Te in the EDX study (Fig. S3B in ESI†) also suggest the formation of GSH-Au_{25}NC-QD nanocomposite. Again the TEM image (Fig. S3C in ESI†) of Cys-Au_{25}NC-QD nanocomposite shows the attachment of CdTe QDs with Cys capped Au NCs and this is further supported by EDX study (Fig. S3D in ESI†).

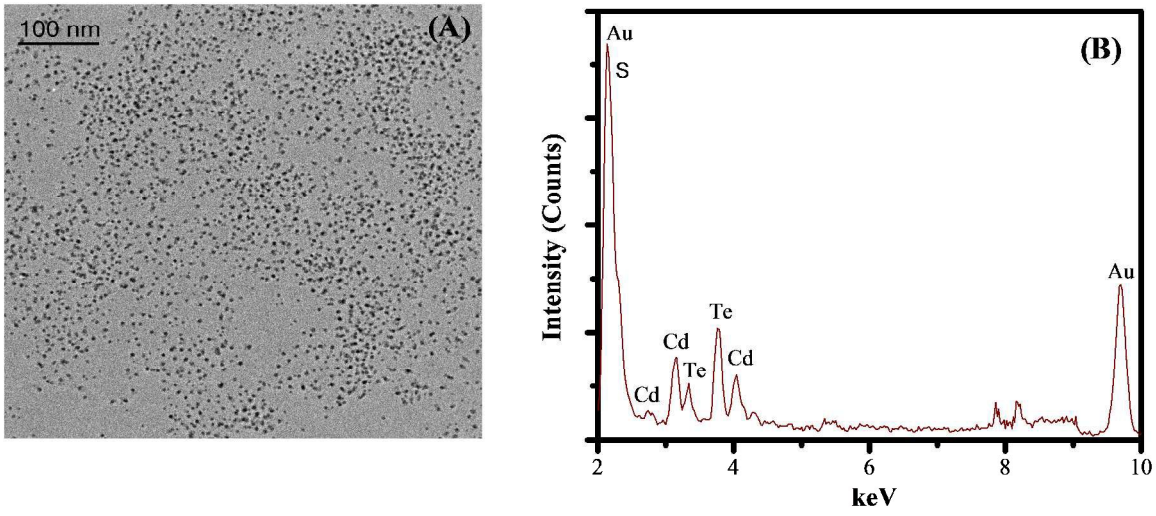

Fig. 6 TEM image (A) and energy dispersive X-ray (EDX) spectra (B) of BSA-Au_{25}NC-QD nanocomposite for Au: Cd ratio 0.16:1.

FTIR syudy is used to investigate the interaction between CdTe QDs and Au NCs in each Nanocomposites (Fig. S4 in ESI†). The vibrations peaks at 2970 cm^{-1} and 2880 cm^{-1} are due to symmetric and asymmetric stretching modes of -CH_2. The vibration frequency at around 1380 cm^{-1} is due to –C-H bending. The peak nearer to 3320 cm^{-1} is due to N-H stretching, assigned as amide A.[36] However, the stretching frequency of N-H bond in these Au NC-QD nanocomposites is shifted around 30 cm^{-1}, indicating the electrostatic interaction between capping ligands of Au clusters with CdTe QDs. However no remarkable change of peaks in fingerprint region is observed.

The steady state and time resolved spectroscopic studies have been used to understand the photophysical interactions between CdTe QDs with Au NCs. In the steady state fluorescence measurement, PL quenching of CdTe QDs is observed in presence of Au NCs for all nanocomposites. The intensity of pure CdTe QDs gradually decreased with increasing the Au: Cd ratio in nanocomposites (Fig. S5 in ESI†).

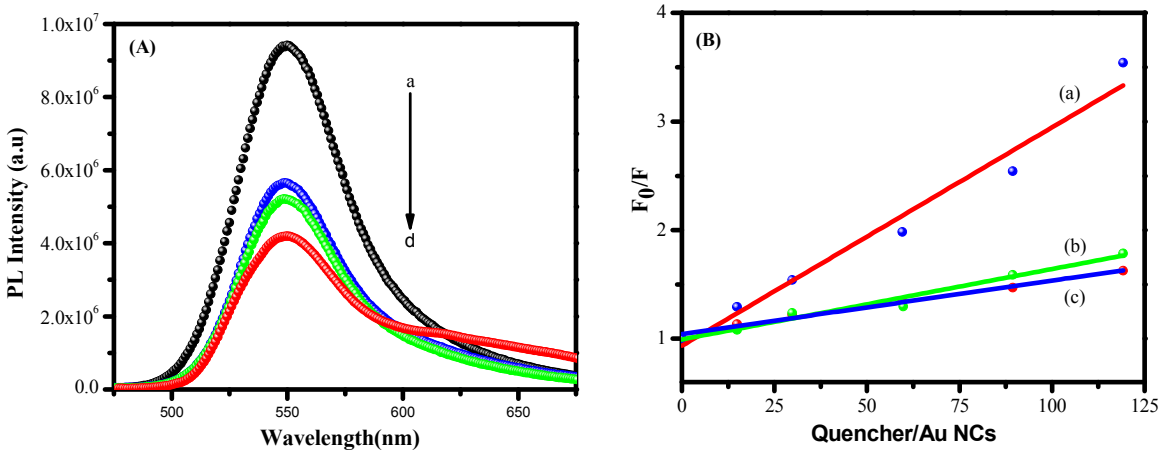

Fig. 7 (A) Photoluminescence spectra of CdTe QDs solution in water without Au NCs (a) and nanocomposites in presence of (b) GSH-Au_{25}NC, (c) Cys-Au_{25}NC, (d) BSA-Au_{25}NC with Au: Cd ratio of 0.16:1, and (B) Stern–Volmer plot of BSA-Au_{25}NC-QD (a), Cys-Au_{25}NC-QD (b) and GSH-Au_{25}NC-QD (c) nanocomposites, respectively.

The photoluminescence (PL) intensity of CdTe QDs is quenched in presence of Au NCs and the rate of PL quenching of CdTe QDs varies with changing the ligand of Au NCs where Au: Cd ratio is 0.16: 1. In GSH-Au_{25}NC-QD nanocomposite, 43% PL quenching of CdTe QDs is observed. The PL quenching of CdTe QDs is found 45 % and 73% for Cys-Au_{25}NC-QD and BSA-Au_{25}NC nanocomposites, respectively (Fig. 7A). Stern-Volmer study is performed to understand the quenching mechanism in different nanocomposites. The Stern-Volmer plot for BSA capped Au NCs is steeper than the Cys and GSH capped Au NCs. The Stern-Volmer constants are evaluated from the slop of the plot, and corresponding Stern-Volmer constants are found to be 4.94 x 10^6, 6.49 x 10^6 and 2.012 x 10^7 M^{-1} for GSH-Au_{25}NC-QD, Cys-Au_{25}NC-QD, and BSA-Au_{25}NC-QD nanocomposite, respectively (Fig. 7B).[48, 49] The Stern-Volmer quenching constant which measures the efficiency of quenching. The higher value quenching rate constants imply the static quenching process which arises due to formation of complex between BSA and Au clusters. The PL quenching of CdTe QDs may be due to energy transfer from CdTe QDs (donor) to Au NCs (acceptor) or other parallel quenching processes. It is interesting to mention that no PL quenching is observed when negatively charged GSH capped CdTe QDs are used to

make composite with negatively charged GSH capped Au NCs, indicating the strong repulsion hinders the PL quenching (Fig. S6 in ESI†).

The exciton dynamics of CdTe QDs in each nanocomposite have been investigated by using time-resolved fluorescence spectroscopy. The decay times of CdTe QDs have been measured in absence and presence of Au NCs and the corresponding decay times of CdTe QDs are given in Table 2.

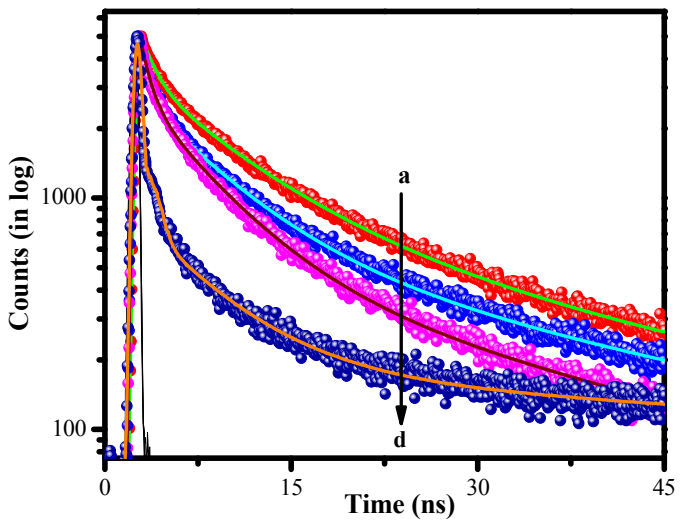

Fig. 8 Time-resolved decay time plots of the pure CdTe QDs without Au NCs (a), GSH-Au_{25}NC-QD (b), Cys-Au_{25}NC-QD (c), and BSA-Au_{25}NC-QD (d) nanocomposite for Au: Cd ratio of 0.16:1, respectively.

The average decay time of pure CdTe QDs is found to be 7.91 ns with the components of 1.07 ns (45%), 7.52 ns (40%), and 29.48 ns (15%). It is interesting to note that the decay time of CdTe QDs is reduced to 5.13 ns with the components of 0.69 ns (61%), 6.37 ns (30%), and 31.15 ns (9%) in GSH-Au_{25}NC-QD nanocomposite for Au: Cd ratio 0.16:1.

Table 2 Time resolved fluorescence data for CdTe QDs and different nanocomposites (emission wavelength fixed at 550 nm).

Au : Cd Ratio	τ_1 in ns (a_1)	τ_2 in ns (a_2)	τ_3 in ns (a_3)	$\langle\tau\rangle$ (in ns)	QY (%)
CdTe-QDs	1.07 (0.45)	7.52 (0.40)	29.48 (0.15)	7.91	1.35
GSH-Au_{25}NC-QD 0.02:1	1.19 (0.49)	7.27 (0.39)	28.81 (0.12)	6.87	1.04
GSH-Au_{25}NC-QD 0.16:1	0.69 (0.61)	6.37 (0.30)	31.15 (0.09)	5.13	0.73
Cys-Au_{25}NC-QD 0.02:1	1.06 (0.50)	6.91 (0.39	27.56 (0.11)	6.25	1.16
Cys-Au_{25}NC-QD 0.16:1	0.72 (0.60)	5.51 (0.32)	25.45 (0.08)	4.23	0.72
BSA-Au_{25}NC-QD 0.02:1	0.54 (0.81)	5.52 (0.15)	38.71 (0.04)	2.81	0.45
BSA-Au_{25}NC-QD 0.16:1	0.32 (0.94)	6.21 (0.05)	71.58 (0.01)	1.32	0.21

Similarly, the decay time of CdTe QDs is reduced to 4.23 ns with the components of 0.72 ns (60%), 5.51 ns (32%), and 25.45 ns (8%) for Cys-Au_{25}NC-QD nanocomposite. Significant change in the decay time of CdTe QDs in BSA-Au_{25}NC-QD nanocomposite is observed and the decay time is found to be to 1.32 ns with the components of 0.32 ns (94%), 6.21 ns (5%), and 71.58 ns (1%) (Fig. 8). The faster component of the decay curves has pronounced change with

changing capping agents. Again, we have measured the decay time of CdTe QDs in different nanocomposite with varying the ratio of Au: Cd. (Fig. S7 in ESI†). Furthermore, we have calculated the quantum yields (QY) of CdTe QDs and respective nanocomposites, data are given in Table 2. The QY of pure CdTe QDs is 1.35% and gradually decreases with increasing the ratio of Au: Cd. The QY of CdTe QDs is reduced to 0.73 % for Au: Cd ratio 0.16:1 in GSH-Au_{25}NC-QD nanocomposites. The QY decreases to 0.72% and 0.21% in Cys-Au_{25}NC-QD and BSA-Au_{25}NC-QD nanocomposite, respectively. For further analysis, the radiative and nonradiative decay rates of CdTe QDs in nanocomposites have been estimated by using the following equation,[40]

$$k_r = \phi / \tau \quad (4)$$

$$k_{nr} = (1-\phi)/ \tau \quad (5)$$

k_r, and k_{nr} represents the radiative, and nonradiative rate constants, respectively. ϕ and τ are the quantum yield and the average decay time of sample, respectively. The radiative and nonradiative rate constants for pure CdTe QDs are found to be 1.70×10^6 sec^{-1} and 1.24×10^8 sce^{-1} respectively. However, the radiative and nonradiative rate constants are found to be 1.42×10^6 sec^{-1} and 1.93×10^8 sec^{-1} for Au: Cd ratio 0.16: 1 in GSH-Au_{25}NC-QD nanocomposite. Similarly for Au: Cd ratio 0.16: 1 in Cys-Au_{25}NC-QD nanocomposite, the radiative and nonradiative rate constants are found to be 1.70×10^6 sce^{-1} and 2.34×10^8 sce^{-1}. Significant change in nonradiative rate constant is observed in case of BSA-Au_{25}NC-QD, which is found to be 7.55×10^8 sec^{-1} for the same ratio of Au: Cd. The change of nonradiative rate constant indicates the energy transfer from CdTe QDs to Au nanocluster cluster. To calculate the efficiency of energy transfer in nanocomposite system, the following equation is used,

$$\phi_{ET} = 1- (\tau_{DA}/ \tau_D) \quad (6)$$

ϕ_{ET}, τ_{DA}, and τ_D represent the efficiency of energy transfer, decay time of donor in presence of acceptor and decay time of donor in absence of acceptor, respectively. Here, we prefer to calculate the efficiency of energy transfer from the change in decay time rather than PL quenching. Because the PL quenching of CdTe QDs in nanocomposites measure the total amount of quenching, not only due to energy transfer. However, the change in the decay time represents the actual amount of energy transfer from CdTe QDs to Au NCs only.[50, 51] The calculated energy

transfer efficiency is found to be 35% for GSH-Au_{25}NC-QD nanocomposite. Similarly ϕ_{ET} for Cys-Au_{25}NC-QD nanocomposite is found to be 46%. Again the corresponding energy transfer efficiency is found to be 83% in BSA-Au_{25}NC-QD nanocomposite. Thus, the rate of energy transfer from CdTe QDs to Au NCs is higher for BSA-Au_{25}NC compared to others. As CdTe QDs and Au NCs both have semiconductor like transition behavior therefore, we have used Förster resonance energy transfer (FRET) mechanism to calculate the donor-acceptor (D-A) distance .[47] Förster distance (R_0) is calculated from the following equation.[40]

$$R_0 = 0.211[k^2\, \eta^{-4}\, \Phi_D J(\lambda)]^{1/6} \text{ (in angstroms)} \qquad (7)$$

Where k^2 is the orientation factor between donor and acceptor. k^2 is generally used 2/3 for random orientation but in this case of both donor and acceptor are rigidly or semi − rigidly fixed in excited states, then k^2 =0.476.[40] Φ_D (1.35%) is the quantum yield of donor, $J(\lambda)$ is the overlap integral between the absorption of acceptor (Au NCs) and emission of donor (CdTe QD), and η (1.33) is the refractive index of the water. The value of overlap integral $J(\lambda)$ has been evaluated by the following equation.

$$J(\lambda) = \frac{\int_0^\infty F_D(\lambda)\varepsilon_A(\lambda)\lambda^4\, d\lambda}{\int_0^\infty F_D(\lambda) d\lambda} \qquad (8)$$

Where $F_D(\lambda)$ is the corrected fluorescence intensity of the donor in range of wavelength λ to λ+Δλ with the total normalized intensity and $\varepsilon_A(\lambda)$ is the extinction coefficient of the acceptor at λ.

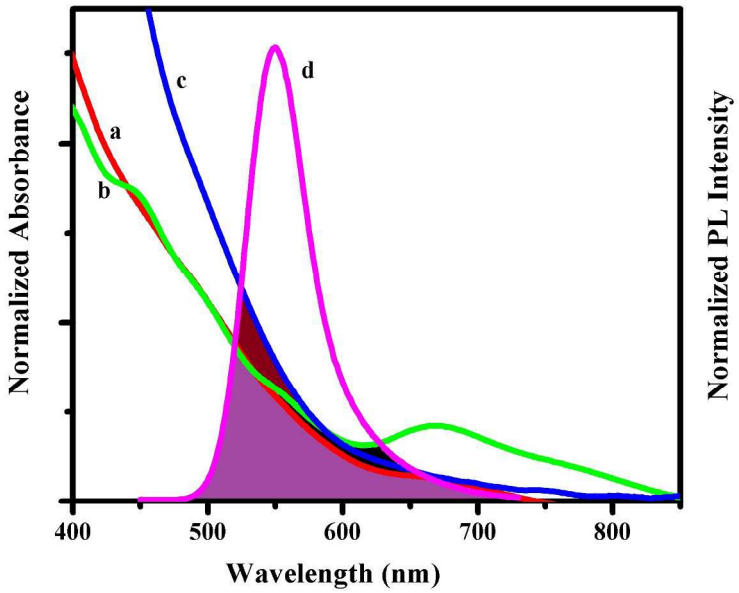

Fig. 9 The overlap plot between the emission spectrum of the CdTe QDs (d) and the absorption spectrum of GSH capped Au NCs (a), Cys capped Au NCs (b), and BSA capped Au NCs (c).

The calculated overlap integral values are found to be 3.17×10^{15}, 3.81×10^{15} and 1.17×10^{16} $M^{-1}cm^{-1}$ nm^4 corresponding to GSH-Au_{25}NC-QD, Cys-Au_{25}NC-QD and BSA-Au_{25}NC-QD nanocomposites, respectively listed in Table 4. The overlap integral plot for BSA-Au_{25}NC-QD, GSH-Au_{25}NC-QD and Cys-Au_{25}NC-QD nanocomposites are given in Fig. 9. Again the overlap integral is related to Förster distance (R_0) by the above equation (7). The R_0 values are found to be 28.83 Å, 29.72 Å and 35.84 Å, GSH-Au_{25}NC-QD, Cys-Au_{25}NC-QD and BSA-Au_{25}NC-QD nanocomposites, respectively (Table 4). The distances between donor and acceptor molecules are calculated by following equation.[40 50]

$$E_{ET} = \frac{R_0^6}{R_0^6 + r^6} \qquad (9)$$

Where E_{ET} is the energy transfer efficiency, r is the experimental distance between donor and acceptor for one donor to one acceptor interaction. For one donor molecule interacts with n independent acceptor molecules at a fixed distance r_n, then the energy transfer efficiency is given by[50]

$$E_{ET} = \frac{nR_0^6}{nR_0^6 + r_n^6} \quad (10)$$

Here, the value of n is estimated by fitting the decay curve using the stochastic kinetic model.

Kinetic Model

To further understand the energy transfer process in QD-Au NC nanocomposites system, we have analyzed the decay curves by using a stochastic kinetic model.[52, 53 54] The quenching of CdTe QDs by Au NCs occurs in competition with unimolecular decay processes of CdTe QDs.

$$QD_n^* \xrightarrow{k_0} QD_n \quad (11)$$

$$QD_n^* \xrightarrow{nk_q} QD_n \quad (12)$$

where QD_n^* stands for excited-state CdTe QDs with n number of Au clusters attached per donor, while QD_n stands for ground state CdTe QDs with n number of Au NCs attached. k_0 is the decay constant due to unimolecular process of the excited state donor in the absence of acceptor, while k_q is the quenching rate constant per one acceptor molecule (due to energy transfer). When one CdTe QD with n number of acceptor molecules is excited, the rate constant of the excited-state decay for that CdTe QD is given by $k_0 + nk_q$, and the total quenching rate constant is nk_q. We also assume that the distribution of the number of Au NCs attached to one CdTe QDs follows a Poisson distribution.[50, 53, 55]

$$\Phi(n) = (m^n/n!) \exp(-m) \quad (13)$$

Where m is the mean number of Au NC attached to per CdTe QD. Therefore, the averaged decay curve of the excited CdTe QD with the mean number of Au NCs attached is given by[53]

$$I(t,m) = I_0 \sum_{n=0}^{\alpha} \Phi(n) \exp[-(k_0 + nk_q)t] \quad (14)$$

Now, along with the acceptor Au NCs, there exist some unidentified traps on the surface of the CdTe QDs, and these are also taken into account. If the distribution of the number of unidentified traps on the surface of CdTe QDs follows a Poisson distribution with the average number (m_t),

the decay curves of the excited state of CdTe QDs in the absence and presence of Au NCs are described by

$$I(t,0) = I_0 \exp\{-k_0 t - m_t[1 - \exp(-k_{qt}t)]\} \quad (15)$$

$$I(t,m) = I_0 \exp\{-k_0 t - m_t[1 - \exp(-k_{qt}t)] - m[1 - \exp(-k_q t)]\} \quad (16)$$

Where k_{qt} is the quenching rate constant by unidentified traps state may be different from that (k_q). The details derivations are given in our previous reports.[56, 57] We have estimated the values of the parametersm_t, k_{qt}, k_0, m, and k_q by fitting equation (15) and (16) to the decay curves of CdTe QDs in the absence and presence of Au NCs (Fig. 10).

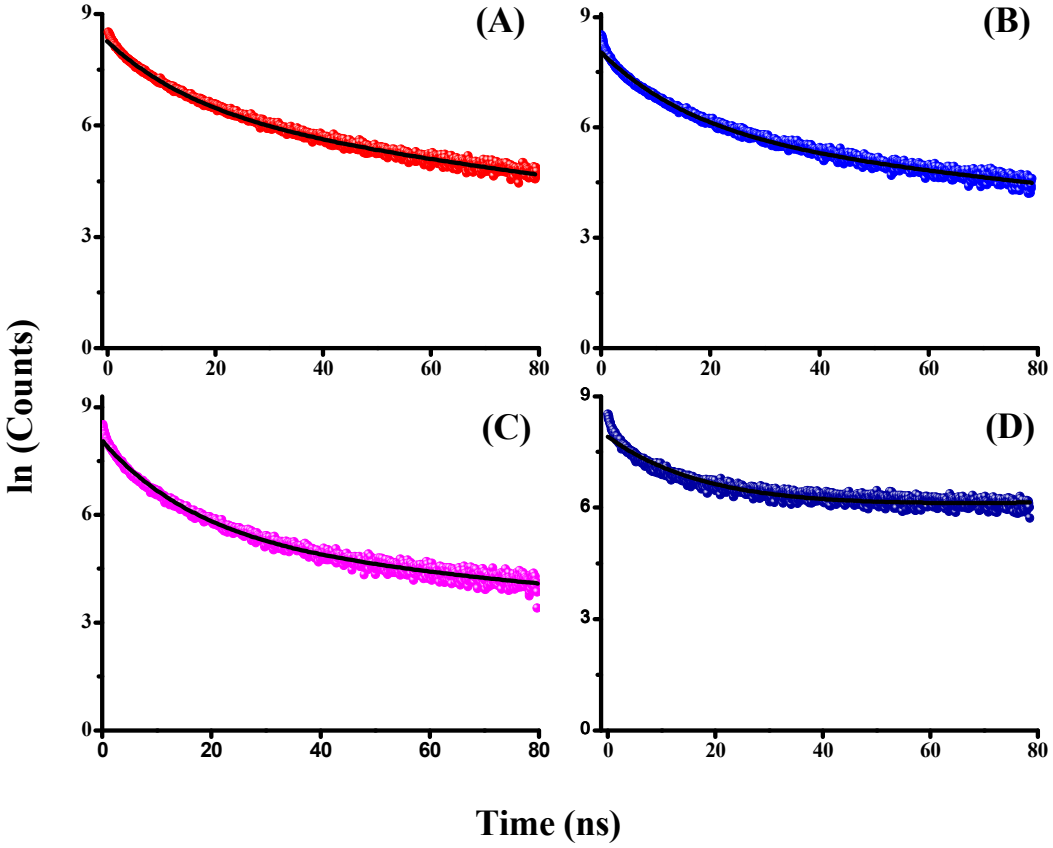

Fig. 10 Time-resolved decay time plot of pure CdTe QDs without Au NCs (A), GSH-Au_{25}NC-QD (B), Cys-Au_{25}NC-QD (C), and BSA-Au_{25}NC-QD (D) nanocomposite for Au: Cd ratio of 0.16:1, respectively. Black curves show the result of fitting the curves with equation 14.

We have fitted the decay curves of CdTe QDs in absence of Au NCs and presence of three different Au NCs by fixing the rate constant (k_0) and observed value of (k_0) is found to be 0.0185 ns^{-1} for pure CdTe QDs and all nanocomposites system. All the fitted results are summarized in Table 3. The calculated values for quenching rate constant (k_q) are found to be 0.0018, 0.00188, 0.00165 ns^{-1} for corresponding nanocomposites. The quenching rate constant (k_{qt}) due to unidentified traps state are the same even after addition of Au NCs because we consider the trap states to be the same. From the Poisson distribution plot (Fig. 10) we have estimated the number of Au NCs (quencher) attached to per CdTe QDs and participating in energy transfer process are 1.80, 2.50, 10.60, respectively. Again Poisson distribution results clarifies how the numbers of Au NCs per CdTe QD varying with changing the capping ligands of Au NCs in nanocomposites. In BSA-Au_{25}NC-QD nanocomposites energy transfer efficiency is highest because more number of BSA capped Au NCs attached to one CdTe QDs.

Table 3 Overview of the values of quenching parameters using the kinetic model

System	k_0 (ns^{-1})	m_t	k_{qt} (ns^{-1})	m	k_q (ns^{-1})
CdTe QDs	0.0185	11.63	0.0550		
GSH-Au_{25}NC-QD	0.0185	13.01	0.0550	1.80	0.00180
Cys-Au_{25}NC-QD	0.0185	15.94	0.0550	2.50	0.00188
BSA-Au_{25}NC-QD	0.0185	11.30	0.0550	10.60	0.00165

The calculated distances (r_n) between donor and acceptor are found to be 35.31 Å, 35.53 Å and 40.81 Å, respectively (Table 4). Interestingly the energy transfer efficiency and the rate of energy transfer order is reverse because in case of BSA-Au_{25}NC-QD nanocomposites more number of BSA-capped Au NCs attached to one CdTe QDs than in other nanocomposites, this claries higher rate of energy transfer.

Table 4 Energy transfer parameters for CdTe QDs and nanocomposites using FRET method.

System (Au: Cd)	$J(\lambda)$ (M^{-1} cm^{-1} nm^4)	R_0 (Å)	r(Å)	r_n(Å)	Energy Transfer (%)	Rate of energy transfer (k_{ET}) in sec^{-1}
GSH-Au_{25}NC-QD (0.16:1)	3.17×10^{15}	28.83	31.96	35.25	35	3.78×10^7
Cys-Au_{25}NC-QD (0.16:1)	3.81×10^{15}	29.72	30.52	35.56	46	4.30×10^7
BSA-Au_{25}NC-QD (0.16:1)	1.17×10^{16}	35.84	27.51	40.78	83	5.82×10^7

Thus, the rate of energy transfer is higher for CdTe QD to BSA capped Au NCs with respect to Cys-capped and GSH-capped Au NCs. According to Förster theory, the rate of energy transfer $[k_{ET}(r_n)]$ is given by following equation.

$$k_{ET}(r_n) = \frac{1}{\tau_D}\left(\frac{R_0}{r_n}\right)^6 \quad (17)$$

The calculated rate of energy transfer from CdTe QDs to Au NCs for three nanocomposites are found to be 3.78×10^7, 4.30×10^7 and 5.82×10^7 sec^{-1} respectively. In most of the cases, the energy transfer from donor to acceptor is discussed as a FRET process. FRET occurs when photo-excited donor fluorophore molecules transferred energy to nearby acceptor molecules. The efficiency of energy transfer increases with increasing the spectral overlap between donor emission and acceptor absorption. The spectral overlapping integral value of BSA-Au_{25}NC-QD nanocomposite is 4-times higher than the overlap integral of GSH-Au_{25}NC-QD nanocomposite which plays an important role on the energy transfer process (Table 4). Again considering, the

Poisson distribution of acceptors on the surface of donor, we have estimated exact numbers of acceptor per donor. Interestingly, the size of all the three Au NCs is same with 25-number of gold atoms at core but the capping ligands are different. The surfaces of Au NCs are capped by three different ligands and the distances between Au NCs (donor) and QDs (acceptor) molecules are totally controlled by the capping ligands of Au NCs. Analysis reveals that photophysical properties i.e. PL quenching, decay time, radiative and nonradiative decay rate and energy transfer process is controlled by the capping ligands of Au NCs.

Conclusion:

In summary, Au NC-QD nanocomposites have been designed through the electrostatic force of interaction between positively charged CdTe QDs and negatively charged Au NCs. Here the core sizes (< 2 nm) of Au NCs are same with 25 numbers of gold atoms but the capping ligands are different. The PL quenching of CdTe QDs is mainly due to the energy transfer from photo excited CdTe QDs to Au NCs. Steady state and time resolve studies reveal the energy transfer from CdTe QDs to Au NCs with different rates. Energy transfer efficiency is found to be 83% in case of BSA capped Au NCs whereas 46% and 35% are for Cys and GSH capped Au NCs. The corresponding rate of energy transfer is observed 3.78×10^7, 4.30×10^7, and 5.82×10^7 sce^{-1}, respectively. A stochastic model has been proposed to quantify the number of donors per acceptor. The energy transfer efficiency increases with increasing the numbers of Au NCs per CdTe QD, which is governed by capping ligands. It reveals that the rate of energy transfer varies with changing the capping agents. Overall, this research work has shed on the light harvesting issue and could have some exciting practical application in the field of advance materials research.

Acknowledgement: "DAE-SRC Outstanding Investigator Award" is gratefully acknowledged for financial support. DB and BP thanks CSIR for awarding fellowship.

Electronic supplementary information (ESI) available. See DOI: 10.1039/x0xx00000x

References:

1 M.-C. Daniel and D. Astruc, *Chem. Rev*., 2004, **104**, 293-346.

2 C. Burda, X. Chen, R. Narayanan and M. A. El-Sayed, *Chem. Rev*., 2005, **105**, 1025-1102.

3 C. J. Murphy, A. M. Gole, S. E. Hunyadi and C. J. Orendorff, *Inorg. Chem.,* 2006, **45**, 7544-7554.

4 C.-C. Huang, Z. Yang, K.-H. Lee and H.-T. Chang, *Angew. Chem., Int. Ed.*, 2007, **46**, 6824-6828.

5 R. C. Triulzi, M. Micic, S. Giordani, M. Serry, W.-A. Chiou and R. M. Leblanc, *Chem. Commun.*, 2006, 5068-5070.

6 G. Wang, T. Huang, R. W. Murray, L. Menard and R. G. Nuzzo, *J. Am. Chem. Soc.*, 2005, **127**, 812-813.

7 R. Jin, S.-K. Eah and Y. Pei, *Nanoscale*, 2012, **4**, 4026-4026.

8 T. Udayabhaskararao and T. Pradeep, *J. Phys. Chem. Lett.*, 2013, **4**, 1553-1564.

9 Y. Yu, Q. Yao, Z. Luo, X. Yuan, J. Y. Lee and J. Xie, *Nanoscale*, 2013, **5**, 4606-4620.

10 K. L. Kelly, E. Coronado, L. L. Zhao and G. C. Schatz, *J. Phys. Chem. B*, 2002, **107**, 668-677.

11 K.-S. Lee and M. A. El-Sayed, *J. Phys. Chem. B*, 2006, **110**, 19220-19225.

12 A. Arbouet, C. Voisin, D. Christofilos, P. Langot, N. D. Fatti, F. Vallée, J. Lermé, G. Celep, E. Cottancin, M. Gaudry, M. Pellarin, M. Broyer, M. Maillard, M. P. Pileni and M. Treguer, *Phys. Rev. Lett.*, 2003, **90**, 177401.

13 M. Zhu, C. M. Aikens, F. J. Hollander, G. C. Schatz and R. Jin, *J. Am. Chem. Soc.*, 2008, **130**, 5883-5885.

14 Y. Negishi, N. K. Chaki, Y. Shichibu, R. L. Whetten and T. Tsukuda, *J. Am. Chem. Soc.*, 2007, **129**, 11322-11323.

15 J. Zheng, C. Zhang and R. M. Dickson, *Phys. Rev. Lett.*, 2004, **93**, 077402.

16 X. Yuan, M. I. Setyawati, A. S. Tan, C. N. Ong, D. T. Leong and J. Xie, *NPG Asia Mater*, 2013, **5**, e39.

17 Y. Negishi, K. Nobusada and T. Tsukuda, *J. Am. Chem. Soc.*, 2005, **127**, 5261-5270.

18 W. GL, H. T, M. RW, M. L and N. RG, *J. Am. Chem. Soc.*, 2005, **127**, 812.

19 M. K. Corbierre and R. B. Lennox, *Chem. Mater.*, 2005, **17**, 5691-5696.

20 Z. J, P. JT and D. RM, *J. Am. Chem. Soc.*, 2003, **125**, 7780.

21 X. Yuan, Z. Luo, Q. Zhang, X. Zhang, Y. Zheng, J. Y. Lee and J. Xie, *ACS Nano*, 2011, **5**, 8800-8808.

22 N. Enkin, E. Sharon, E. Golub and I. Willner, *Nano Lett.*, 2014, **14**, 4918-4922.

23 N. Enkin, F. Wang, E. Sharon, H. B. Albada and I. Willner, *ACS Nano*, 2014, **8**, 11666-11673.

24 N. Goswami, A. Giri, M. S. Bootharaju, P. L. Xavier, T. Pradeep and S. K. Pal, *Anal. Chem.*, 2011, **83**, 9676-9680.

25 E. Sharon, N. Enkin, H. B. Albada and I. Willner, *Chem. Commun.*, 2015, **51**, 1100-1103.

26 L. Shang, N. Azadfar, F. Stockmar, W. Send, V. Trouillet, M. Bruns, D. Gerthsen and G. U. Nienhaus, *Small*, 2011, **7**, 2614-2620.

27 F. Aldeek, M. A. H. Muhammed, G. Palui, N. Zhan and H. Mattoussi, *ACS Nano*, 2013, **7**, 2509-2521.

28 M. A. H. Muhammed, F. Aldeek, G. Palui, L. Trapiella-Alfonso and H. Mattoussi, *ACS Nano*, 2012, **6**, 8950-8961.

29 Z. Wu and R. Jin, *Nano Lett.*, 2010, **10**, 2568-2573.

30 Y.-S. Chen and P. V. Kamat, *J. Am. Chem. Soc.*, 2014, **136**, 6075-6082.

31 S. Antonello, G. Arrigoni, T. Dainese, M. De Nardi, G. Parisio, L. Perotti, A. René, A. Venzo and F. Maran, *ACS Nano*, 2014, **8**, 2788-2795.

32 J. Zhang, Y. Tang, K. Lee and M. Ouyang, *Nature*, 2010, **466**, 91-95.

33 K. K. Haldar, N. Pradhan and A. Patra, *Small*, 2013, **9**, 3424-3432.

34 T. Pons, I. L. Medintz, K. E. Sapsford, S. Higashiya, A. F. Grimes, D. S. English and H. Mattoussi, *Nano Lett.*, 2007, **7**, 3157-3164.

35 J. Xie, Y. Zheng and J. Y. Ying, *J. Am. Chem. Soc.*, 2009, **131**, 888-889.

36 B. Paramanik, S. Bhattacharyya and A. Patra, *Chem.- Eur. J.*, 2013, **19**, 5980-5987.

37 X. Wang and X. Guo, *Analyst*, 2009, **134**, 1348-1354.

38 S. Kundu, S. Sadhu, R. Bera, B. Paramanik and A. Patra, *J. Phys. Chem. C*, 2013, **117**, 23987-23995.

39 W. W. Yu, L. Qu, W. Guo and X. Peng, *Chem. Mater.*, 2003, **15**, 2854-2860.

40 Lakowicz, J. R. *Principles of Fluorescence Spectroscopy;* Springer, 2006; Vol. 1.

41 X. Yuan, B. Zhang, Z. Luo, Q. Yao, D. T. Leong, N. Yan and J. Xie, *Angew. Chem., Int. Ed.*, 2014, **53**, 4623-4627.

42 B. Paramanik and A. Patra, *J. Mater.Chem. C*, 2014, **2**, 3005-3012.

43 T. Das, P. Ghosh, M. S. Shanavas, A. Maity, S. Mondal and P. Purkayastha, *Nanoscale*, 2012, **4**, 6018-6024.

44 B. Jana, S. Bhattacharyya and A. Patra, *Phys. Chem. Chem. Phys.*, 2015, **17**, 15392-15399.

45 T. Sen and A. Patra, *J. Phys. Chem. C*, 2012, **116**, 17307-17317.

46 E. C. Dreaden, A. M. Alkilany, X. Huang, C. J. Murphy and M. A. El-Sayed, *Chem. Soc. Rev.*, 2012, **41**, 2740-2779.

47 F. Aldeek, X. Ji and H. Mattoussi, *J. Phys. Chem. C*, 2013, **117**, 15429-15437.

48 S. Mandal, M. Rahaman, S. Sadhu, S. K. Nayak and A. Patra, *J. Phys. Chem. C*, 2013, **117**, 3069-3077.

49 B. Paramanik, S. Bhattacharyya and A. Patra, *J. Lumin.*, 2013, **134**, 401-407.

50 G. Beane, K. Boldt, N. Kirkwood and P. Mulvaney, *J. Phys. Chem. C*, 2014, **118**, 18079-18086.

51 A. J. Morris-Cohen, V. Vasilenko, V. A. Amin, M. G. Reuter and E. A. Weiss, *ACS Nano*, 2012, **6**, 557-565.

52 E. Zenkevich, F. Cichos, A. Shulga, E. P. Petrov, T. Blaudeck and C. von Borczyskowski, *J. Phys. Chem. B*, 2005, **109**, 8679-8692.

53 S. Sadhu, K. K. Haldar and A. Patra, *J. Phys. Chem. C*, 2010, **114**, 3891-3897.

54 M. Tachiya, *J. Chem. Phys.*, 1982, **76**, 340-348.

55 E. I. Zenkevich, A. P. Stupak, D. Kowerko and C. v. Borczyskowski, *Chem. Phys.*, 2012, **406**, 21-29.

56 S. Sadhu and A. Patra, *J. Phys. Chem. C*, 2012, **116**, 15167-15173.

57 S. Sadhu and A. Patra, *J. Phys. Chem. C*, 2011, **115**, 16867-16872.

TOC: